Resolving the roles of immunity, pathogenesis and immigration for rabies persistence in vampire bats

Supporting Online Material

JC Blackwood, DG Streicker, S Altizer & P Rohani

Contents:

S1 Seroprevalence data

The data figure in the main text (Fig. 1) captures two important aspects of the data: (*I*) seroprevalence by region, and (*II*) relative sample size for each observation. The latter is necessary to identify artificially high or low seroprevalences that result from small sample sizes. Table S1 displays the year, sampling dates, seroprevalence, and number of samples for each study site. Importantly, we note that sample dates ranged from April to August, and seropositive bats are identified in each of these months. The presence of seropositive bats in all regions in all sampled months indicates that the observations are likely not the result of isolated epizootics (as observed in Figs. 3A and 3C in the main text), and instead seropositive bats are consistently found throughout the year.

S2 Estimation of seasonal birth rate

Seasonality has been observed in vampire bat births; for example, an increase in number of births during the wet season was suggested by [16]. This observation was also made in Argentina, with a greater percentage of lactating females and a lower percentage of pregnant females during the wet season [9]. Assuming that increased lactation is correlated with the number of females that recently gave birth, we estimate seasonal birth rates by fitting a cosine function to the data provided in [9]. Specifically, the cosine function takes the form:

$$r(t) = b + A\cos\left(2\pi(t-\phi)/365\right) \tag{S1}$$

where $r(t)$ is the daily birth rate. The data is given in terms of percent of females lactating which provides an indicator of the timing of females giving birth, and we fit the above function to the data using nonlinear least squares, arriving at:

$$r(t) = 26.6581 + 16.4565\cos\left(2\pi(t-32.6747)/365\right). \tag{S2}$$

Finally, this is rescaled so that the mean birth rate is given by one pup per female per year (assuming a 1:1 sex ratio), or $\overline{r} = 0.5/365$ [15]. We arrive at the estimation:

$$r(t) = 0.5/365 + 8.4563 * 10^{-4}\cos\left(2\pi(t-32.6747)/365\right). \tag{S3}$$

Fig S1 displays these results.

S3 Methods for parameter estimation

Table S2 displays all model parameters, descriptions, and known values. In this section we describe our methodology for estimating the parameters $\theta = (\beta_N, \beta_R, \alpha, \phi)$ where β_N and β_R are the transmission rates from infectious bats that have not yet developed clinical rabies and clinically rabid bats, respectively, α is the probability of developing lethal infection upon exposure,

Table S1. Field data

SITE	DEPARTMENT	PROVINCE	YEAR	SAMPLING DATES	SEROPREV	SAMPS
API1	Apurimac	Chincheros	2007	7/17	0	12
			2009	5/18-21	0	19
			2010	8/30,31, 9/1	0.179	28
API4	Apurimac	Chincheros	2007	7/19	0.250	4
API3	Apurimac	Chincheros	2007	7/18	0.238	21
			2010	9/2	0.065	31
API9	Apurimac	Chincheros	2007	8/1	0.222	18
			2009	5/12-15	0.056	18
			2010	8/25-28	0.070	43
API13	Apurimac	Abancay	2009	5/26-29	0.129	62
			2010	9/6-8	0.385	13
API138	Apurimac	Aymaraes	2010	9/9	0	4
API140	Apurimac	Aymaraes	2010	9/10	0.067	30
CAJ01	Cajamarca	Chota	2009	6/30, 7/2-4	0.074	68
			2010	6/30, 7/2-4	0.032	94
CAJ02	Cajamarca	Cutervo	2009	6/18-21	0.085	47
			2010	7/9,11,12	0.069	102
CAJ03	Cajamarca	Cutervo	2009	6/25-28	0.111	9
			2010	7/6-8	0	22
CAJ04	Cajamarca	San Ignacio	2010	7/14/10	0.222	18
LMA10	Lima	Huaral	2007	8/3	0.5	4
			2009	4/22-24	0	36
			2010	5/25, 6/21-23	0.098	51
LMA4	Lima	Caete	2007	7/31	0	2
			2009	4/20,21, 6/3,4	0.364	11
			2010	8/19-21	0.130	23
LMA5	Lima	Barranca	2007	8/1	0.333	15
			2009	5/7-9	0	8
			2010	5/21	0.227	22
LMA6	Lima	Huaura	2007	8/2	0.217	23
			2009	5/4-6	0.023	44
			2010	5/17-20	0.157	102
LMA8	Lima	Huaral	2007	8/2	1	1
			2009	4/27	0.250	12
			2010	5/24	0	2
MDD134	Madre de Dios	Tambopata	2007	7/23	0	3
			2008	7/15,22,23,25,26,28,29, 8/8	0.053	19
			2009	7/27, 10/9,10,13-15,24	0.067	15
			2010	8/6-8,15	0	6
MDD130	Madre de Dios	Manu	2009	6/20, 7/16,17,21 10/17,19,20	0.067	15
			2010	8/11-14	0.143	7

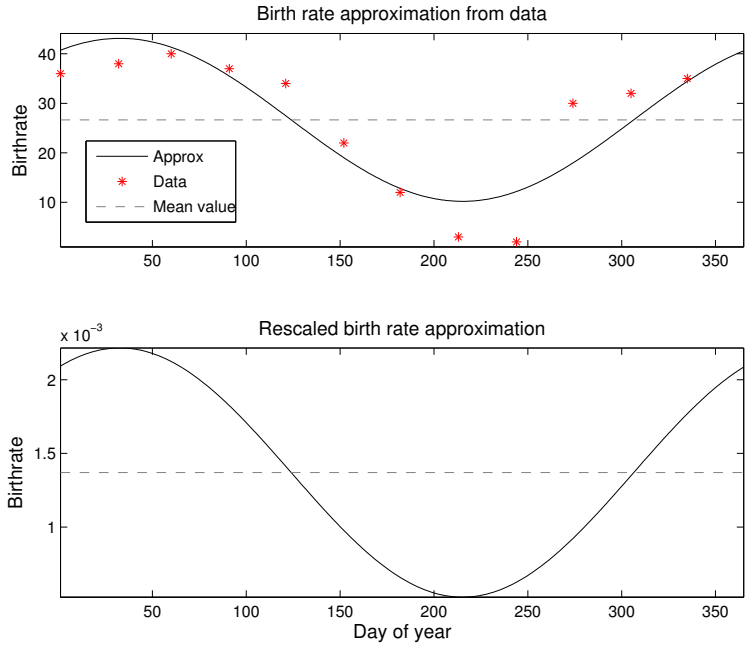

Figure S1. Estimate of seasonal births

and ϕ is the contribution of immigration to the force of infection. We imposed the restriction that $0.05 \leq \alpha \leq 0.85$ as suggested by current estimates ([1, 2, 3]), and we additionally imposed the restriction that $0 \leq R_0 \leq 3$. For each site we assumed that the initial population size is given by the mean of the field estimates between 2007 and 2010, where the field estimates were found using standard capture-recapture methods [11]. Further, colony sizes vary by region, so we simply defined the carrying capacity in each region as the largest colony observed between 2007 and 2010. Further, we note that our analysis assumed independence between sites. However, sites were intentionally spaced at least 20km apart to avoid mixing of bats between sampled colonies. To further justify this assumption, we performed Mantel tests of the association between geographic distance and seroprevalence between sites. This was tested both at the national scale and within a region, and in all cases there is no statistical significance with associated p-values of > 0.05.

Our estimation work utilized particle filtering, implemented from the POMP 0.36-1 package of the statistical computing language R [4, 5]. After implementing fully stochastic versions of our models using the τ-leap method (an approximation to Gillespie's algorithm) [6, 7, 8], we used particle filtering to perform a grid search over all parameters θ and compute the log likelihood at each point. A grid search algorithm was used not only to identify the maximum likelihood estimate (MLE), but to characterize relationships between parameters and parameter sensitivities. We conducted a grid search over α and ϕ and for each parameter combination we find the likelihood by maximizing the likelihood over β_N and β_R. In other words, we first defined a 2-dimensional grid over α and ϕ. For each fixed combination of these two parameters, we then performed a grid search over

all plausible transmission parameters β_N and β_R. The associated maximum likelihood estimate for β_H and β_R is then defined as the likelihood estimate for that fixed α and ϕ. This output is then used to produce the contour plot in Fig. 3 in the main text as well as the contour plots below.

To estimate the likelihood for each parameter set θ, particle filtering requires specification of the "process" model that describes the true transmission dynamics within a single bat colony and an "observation" model that relates model variables to field data. The process model is given by our transmission models, and we assumed that the field data follow a binomial distribution so that for a given study site s and sample date t, the number of seropositive individuals k is given by

$$k \sim \text{Bin}(n, p)$$

where n is the number of samples collected, and p is the seroprevalence predicted by the process model for a given parameter set θ. For each plausible parameter set θ, given a site s we used 2500 particles to first run out transient dynamics resulting from our choice of initial conditions for 5 years and then computed the conditional likelihood at each associated sample time t (i.e. $\mathcal{L}_t^s(\theta)$). The likelihood for a given site is given by the product of the conditional likelihoods, or the sum of the conditional log likelihoods:

$$\log \mathcal{L}^s(\theta) = \sum_{t=1}^{d} \log \mathcal{L}_t^s(\theta).$$

where d is the number of sample dates for a given site s. For each region, we then compute the total log likelihood by summing over each site within that region so that

$$\log \mathcal{L}_{\mathcal{R}}(\theta) = \sum_{s=1}^{q} \log \mathcal{L}^s(\theta)$$

where q is the number of sites in the given region. Finally, the log likelihood at the national level is simply given by the sum over all regions, or

$$\log \mathcal{L}_{\mathcal{T}}(\theta) = \sum_{R=1}^{4} \log \mathcal{L}_{\mathcal{R}}(\theta).$$

S4 Full model descriptions & results

In this section, we completely describe each model for rabies transmission dynamics as proposed in the main text:

(I) *Temporary immunity & lethal infection*. Following exposure to VBRV, bats may either develop temporary immunity or acquire a non-immunizing infection that is always lethal.

(II) *Recovery from infectious states*. Although controversial, evidence from experimentally infected vampire bats suggests that some bats may transiently excrete virus in their saliva prior to recovery [2]. We therefore considered a scenario similar to model I but with a small proportion of infectious bats recovering to acquire temporary immunity.

Table S2. Model parameters

PARAMETER	DESCRIPTION	VALUE	Source
$r(t)$	Seasonal birth rate	See section S2	[9, 10]
K	Carrying capacity	Varies by region	[11]
$1/\epsilon$	Mean duration of time in T class	4.5 months	[12, 13]
$1/\tau_1$	Mean duration of time in E class	21 days	[1]
$1/\tau_2$	Mean duration of time in I_N class	5.78 days	[1]
$1/\delta$	Mean duration of time in I_R class	6 days	[1]
$1/\mu$	Average lifespan	3.4 years	[14, 15]
β_N	Transmission rate from bats in I_N class	Estimated	–
β_R	Transmission rate from bats in I_R class	Estimated	–
α	Probability of infection given exposure	Estimated	–
ϕ	Contribution of immigration to FOI	Estimated	–
c *	Strength of immune boosting	Estimated	–
ρ †	Probability of succumbing to infection	Estimated	–

*Model III only
† Model II only

(III) *Immune boosting*. Experimental evidence from big brown bats (*Eptesicus fuscus*) suggests that repeat exposure to rabies virus could boost a bat's immune response, thus extending the duration of the protected period [17]. We therefore considered a model in which re-exposure depends on the presence of infectious bats, as measured by the *per capita* infection hazard (i.e. the force of infection).

(IV) *Lifelong immunity*. As in model I, but immunity following exposure is lifelong.

Each model assumes that bats either develop immunity or acquire a lethal, non-immunizing infection upon exposure. Challenge studies have been conducted in vampire bats, and in all studies that included serology, some proportions of bats seroconverted as evidenced by production of rabies virus neutralizing antibodies (VNAs) and survived. The proportion of bats that survived is dose dependent. Given that VNAs are considered the gold standard for protection against rabies following vaccination in humans or domestic animals, it is likely that the animals that seroconvert and survive have some degree of protection. Given that bats can live many years in captivity, it has been impossible to discern whether these antibodies give lifelong immunity; therefore, we consider scenario IV in which immunity is lifelong.

For each model, a contour map of the likelihoods for infection probability α versus the effect of immigration ϕ is provided in addition to sample simulations from qualitatively different regions of the contour plot. In a later section, we describe the results for our estimates of β_H and β_R.

Model I (temporary immunity & lethal infection) assumes that a proportion of exposed individuals (α) acquires infection and rabies infection is always lethal. The proportion of individuals

that do not develop clinical rabies $(1-\alpha)$ enter a state with temporary immunity and re-enter the susceptible class at a rate ϵ:

$$\begin{aligned}
\frac{dS}{dt} &= r(t)N(1-\frac{N}{K}) - (\beta_N I_N/N + \beta_R I_R/N + \phi)S + \epsilon T - \mu S && \text{(S4)}\\
\frac{dE}{dt} &= (\beta_N I_N/N + \beta_R I_R/N + \phi)S - (\tau_1 + \mu)E && \text{(S5)}\\
\frac{dT}{dt} &= (1-\alpha)\tau_1 E - (\epsilon + \mu)T && \text{(S6)}\\
\frac{dI_N}{dt} &= \alpha\tau_1 E - (\tau_2 + \mu)I_N && \text{(S7)}\\
\frac{dI_R}{dt} &= \tau_2 I_N - (\delta + \mu)I_R && \text{(S8)}
\end{aligned}$$

The first alternative model that we propose, model II, allows for some individuals that are infectious but have not yet developed clinical rabies (i.e. I_N bats) to recover. Specifically, this model assumes that a fraction $1-\rho$ of I_N bats may develop temporary immunity and subsequently re-enter the susceptible class. To determine the best estimate of $1-\rho$, we use particle filtering as described in previous sections to create a profile likelihood over $1-\rho$, where $0 \leq 1-\rho \leq 0.5$ (Figure S2). Surprisingly, the profile is very flat, with the 95% CI encompassing all values. The MLE corresponds to $1-\rho = 0.3$, or 30% of infectious individuals cannot recover. This value is used for the remainder of the analysis.

$$\begin{aligned}
\frac{dS}{dt} &= r(t)N(1-\frac{N}{K}) - (\beta_N I_N/N + \beta_R I_R/N + \phi)S + \epsilon T - \mu S && \text{(S9)}\\
\frac{dE}{dt} &= (\beta_N I_N/N + \beta_R I_R/N + \phi)S - (\tau_1 + \mu)E && \text{(S10)}\\
\frac{dT}{dt} &= (1-\alpha)\tau_1 E + (1-\rho)\tau_2 I_N - (\epsilon + \mu)T && \text{(S11)}\\
\frac{dI_N}{dt} &= \alpha\tau_1 E - (\tau_2 + \mu)I_N && \text{(S12)}\\
\frac{dI_R}{dt} &= \rho\tau_2 I_N - (\delta + \mu)I_R && \text{(S13)}
\end{aligned}$$

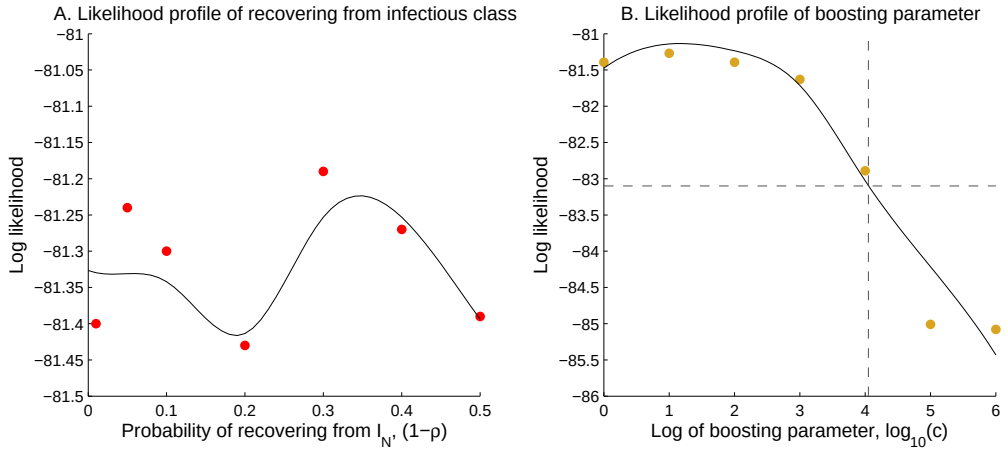

Figure S2. (**A**) Profile likelihood of $1-\rho$, the probability of developing temporary immunity after entering the infectious class, I_N. The 95% CI encompasses all values of $1-\rho$. (**B**) Profile likelihood of the strength of immune boosting, c, plotted on a log scale. The 95% CI is found using the likelihood ratio test, and the vertical dashed line represents the upper bound of the 95% CI and all values within the CI lie above the horizontal line. Here, the 95% CI contains lower values of c. In each plot, for several values of $1-\rho$ and c the corresponding maximum likelihood estimate is displayed. In (**A**) the likelihood surface is very flat over all tested values. The flat profile will likely remain flat if we extend this plot to even higher values of $1-\rho$, but these scenarios are biologically unrealistic. In (**B**) this model approaches the case of lifelong immunity as c increases so that the log likelihood decreases as c increases.

In the second alternative model, model III, we propose that the temporary immunity may be boosted. We make the simple assumption that as the force of infection increases, the rate that individuals return to the susceptible class is slowed. This results in the following model:

$$\frac{dS}{dt} = r(t)N(1-\frac{N}{K}) - (\beta_N I_N/N + \beta_R I_R/N + \phi)S + e^{(-c\lambda)}T - \mu S \quad \text{(S14)}$$

$$\frac{dE}{dt} = (\beta_N I_N/N + \beta_R I_R/N + \phi)S - (\tau_1 + \mu)E \quad \text{(S15)}$$

$$\frac{dT}{dt} = (1-\alpha)\tau_1 E - (\epsilon e^{(-c\lambda)} + \mu)T \quad \text{(S16)}$$

$$\frac{dI_N}{dt} = \alpha\tau_1 E - (\tau_2 + \mu)I_N \quad \text{(S17)}$$

$$\frac{dI_R}{dt} = \tau_2 I_N - (\delta + \mu)I_R \quad \text{(S18)}$$

The constant c indicates a measure of the strength of immune boosting and we again find the profile likelihood over c to determine its MLE, which corresponds to 10 (Figure S2).

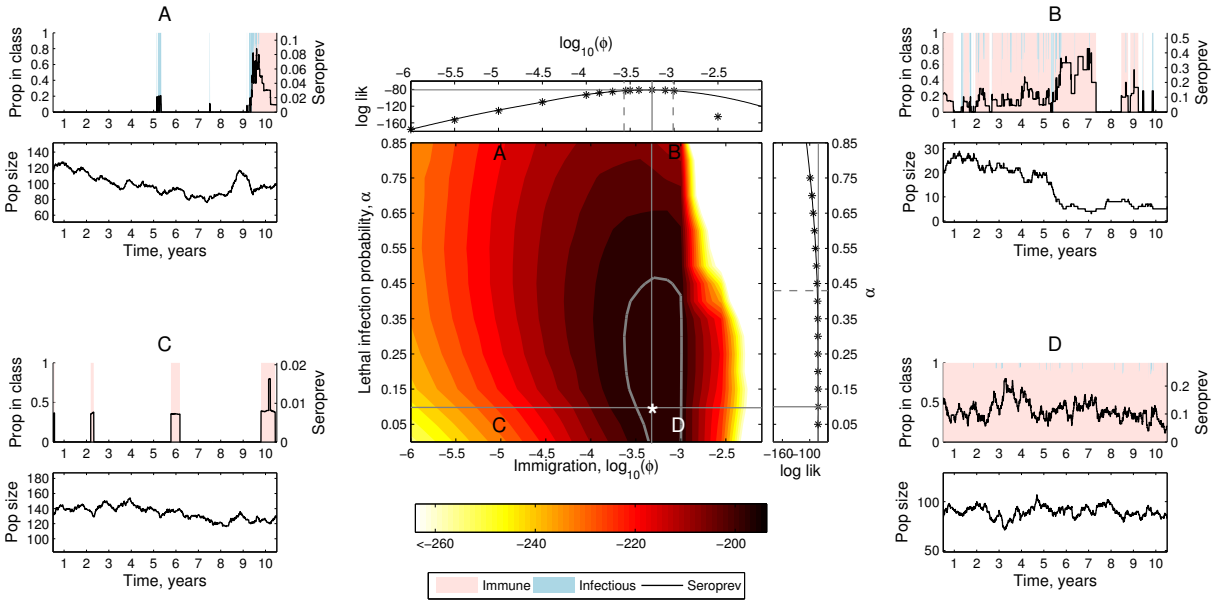

Figure S3. Contour plot of the log likelihood of infection probability α versus the effects of immigration ϕ when infectious but clinically healthy bats (class I_N) can recover (model II). This plot uses $\rho = 0.30$, or on average 30% of bats recover. Parameters for sample simulations: (top left) $\alpha = 0.85$, $\phi = 10^{-5}$, (top right) $\alpha = 0.85$, $\phi = 10^{-3}$, (bottom left) $\alpha = 0.05$, $\phi = 10^{-5}$, (bottom right) $\alpha = 0.05$, $\phi = 10^{-3}$. Shading indicates the proportion of seropositive individuals with temporary immunity (T, light red) and proportion of seropositive individuals that are infectious ($I_N + I_R$, light blue).

In the final model, model IV, we propose that individuals that do not become infectious following exposure develop permanent immunity, or

$$\frac{dS}{dt} = r(t)N(1 - \frac{N}{K}) - (\beta_N I_N/N + \beta_R I_R/N + \phi)S - \mu S \tag{S19}$$

$$\frac{dE}{dt} = (\beta_N I_N/N + \beta_R I_R/N + \phi)S - (\tau_1 + \mu)E \tag{S20}$$

$$\frac{dT}{dt} = (1 - \alpha)\tau_1 E - \mu T \tag{S21}$$

$$\frac{dI_N}{dt} = \alpha\tau_1 E - (\tau_2 + \mu)I_N \tag{S22}$$

$$\frac{dI_R}{dt} = \tau_2 I_N - (\delta + \mu)I_R \tag{S23}$$

As discussed in the main text, this model exhibits differences in the parameter estimates and corresponding confidence intervals compared to the other models. However, the intrinsic R_0 remains less than one which demonstrates that immigration still plays a fundamental role in driving long-term viral persistence. Figure S5 highlights the differences through sample simulations. In this model, regardless of infection probability α, viral persistence is maintained via immunizing, non-lethal exposures (i.e., 'abortive' infections). This is a direct result of the assumption of lifelong immunity. The optimal ϕ is also lower than that found in the previous models because higher immigration levels result in overestimates of the true seroprevalence. Again, we emphasize that based on the MLE this model provides a much less plausible explanation of the data.

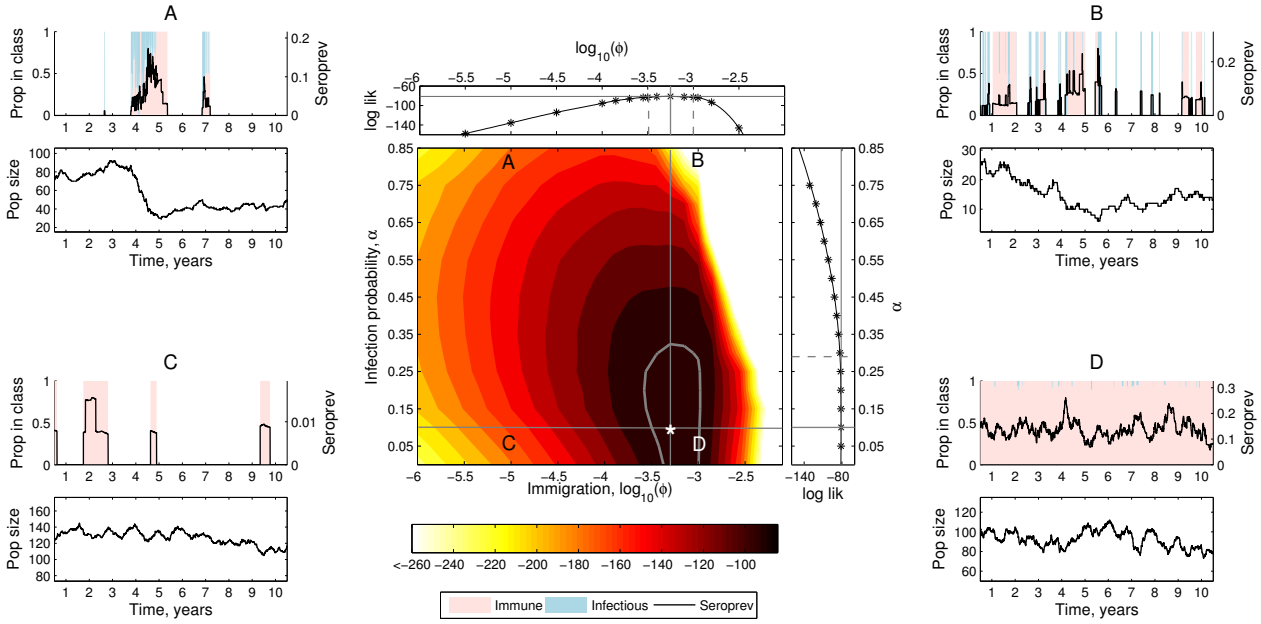

Figure S4. Contour plot of the log likelihood of infection probability α versus the effects of immigration ϕ when immune boosting may occur (model III). Parameters for sample simulations: (top left) $\alpha = 0.85$, $\phi = 10^{-5}$, (top right) $\alpha = 0.85$, $\phi = 10^{-3}$, (bottom left) $\alpha = 0.05$, $\phi = 10^{-5}$, (bottom right) $\alpha = 0.05$, $\phi = 10^{-3}$. Shading indicates the proportion of seropositive individuals with temporary immunity (T, light red) and proportion of seropositive individuals that are infectious ($I_N + I_R$, light blue).

S4.1 Maximum likelihood estimates

Here we present MLE for each of our four competing models (Table S3). As discussed above, models I-III have similar MLEs and confidence bounds, indicating that a high value of ϕ with a corresponding low value of α is essential for the model to accurately represent the observed data. This is independent of the underlying immune mechanisms for these models. Further, we note that $\alpha > 0$, so while this is a lower bound for some model estimates, the CI does not include the value 0.

We tested values of the probability of recovering from infection ($1 - \rho$) in model II ranging from 0-50%, each of which fall in the 95% CI. In other words, the effect of parameters α and ϕ are much more critical in the underlying dynamics. Further, for model III the MLE corresponds to $c = 10$ with an associated total boosting coefficient ($e^{-c\lambda}$) that is very close to one, essentially collapsing back to model I. As the value of c becomes large, model III then approaches the model with lifelong immunity, thereby decreasing the likelihood.

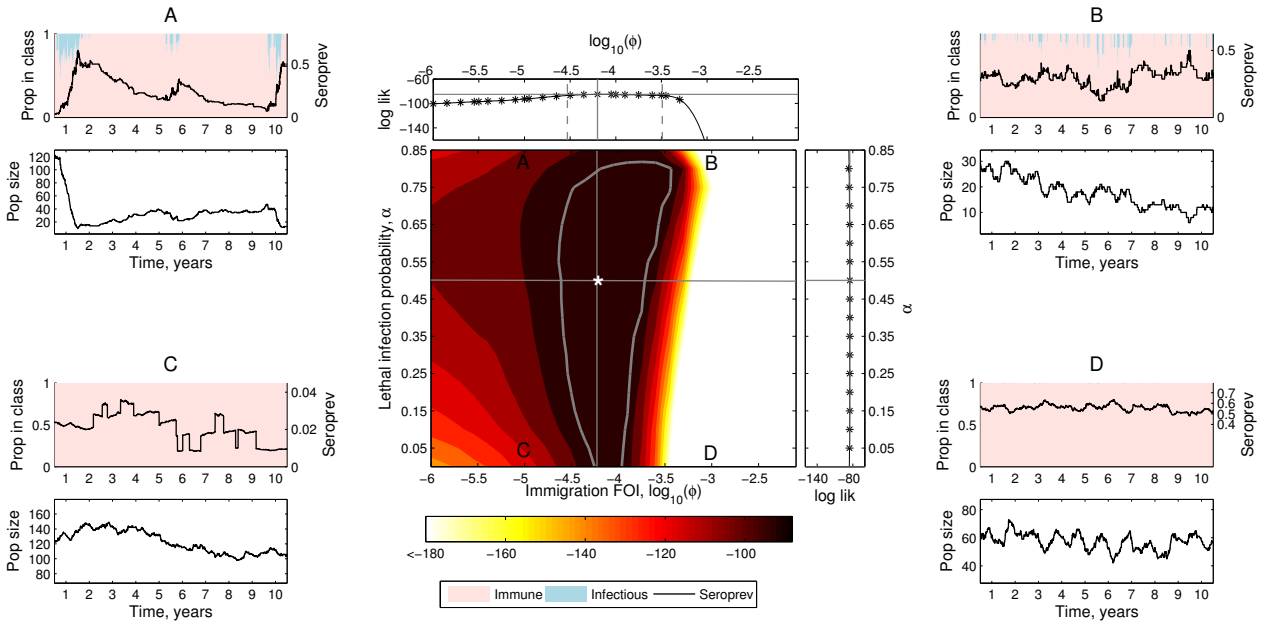

Figure S5. Contour plot of the log likelihood of infection probability α versus the effects of immigration ϕ when acquired immunity is lifelong (model IV). Parameters for sample simulations: (top left) $\alpha = 0.85$, $\phi = 10^{-5}$, (top right) $\alpha = 0.85$, $\phi = 10^{-3}$, (bottom left) $\alpha = 0.05$, $\phi = 10^{-5}$, (bottom right) $\alpha = 0.05$, $\phi = 10^{-3}$. Shading indicates the proportion of seropositive individuals with temporary immunity (T, light red) and proportion of seropositive individuals that are infectious ($I_N + I_R$, light blue).

Table S3. Maximum likelihood estimates

MODEL	PARAMETER	DESCRIPTION	VALUE & 95% CI
I	α	Lethal infection probability	$0.1(0, 0.29)$
	ϕ	Contribution of immigration to FOI	$10^{-3.25}(10^{-3.51}, 10^{-2.83})$
II	α		$0.1(0, 0.43)$
	ϕ		$10^{-3.25}(10^{-3.57}, 10^{-3.01})$
	$1-\rho$	Probability of recovering from infection	$0.3(0, 0.5)$
III	α		$0.1(0, 0.29)$
	ϕ		$10^{-3.25}(10^{-3.53}, 10^{-3})$
	c	Strength of immune boosting	$10(1, 10^{4.05})$
IV	α		$0.5(0, 0.89)$
	ϕ		$10^{-4.2}(10^{-4.53}, 10^{-3.49})$

S4.2 Regional results

In addition to finding the MLE for our model over all sites within Peru, we also found the MLE at the regional scale. In this section we briefly describe the regional results using the model with lethal infection and temporary immunity. The data is separated by administrative department in Peru, and we number them as follows:

A1 Apurimac (Andes, 6 sites)

A2 Cajamarca (Andes, 4 sites)

A3 Lima (Coast, 5 sites)

A4 Madre de Dios (Amazon, 2 sites)

where number of sites sampled within that department as well as the region of Peru the department is located are in parentheses. Figure S6 displays a contour plot of the likelihood values for infection probability, α, versus contribution of immigration to the force of infection, ϕ. Interestingly, the regional results closely match those found at the national level: there is a tradeoff between α and ϕ, with the maximum likelihood values corresponding to a low infection probability with high immigration. The corresponding 95% CIs are much larger than that observed in Figure S6, and this is simply because fewer sites are sampled at the regional level when compared to the national level, resulting in flatter likelihood surfaces.

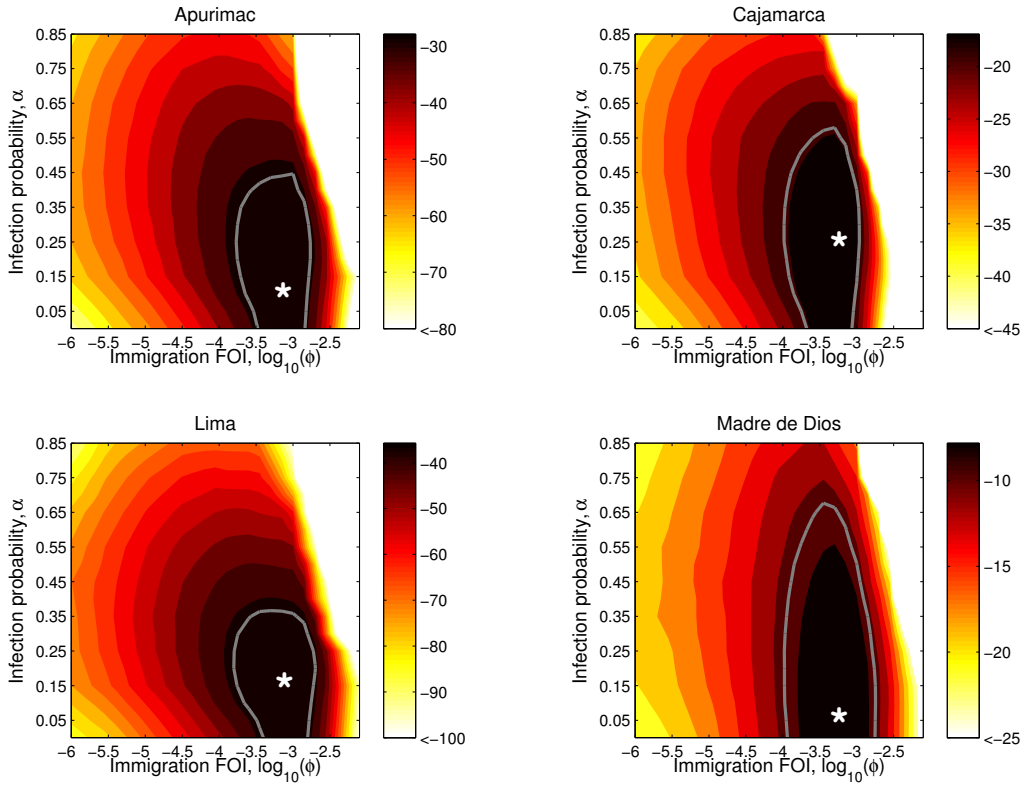

Figure S6. Likelihood of infection probability versus effect of immigration for 4 departments in Peru. White star corresponds to the maximum likelihood estimates: $(\alpha, \phi) = (0.05, 10^{-3.1}), (0.25, 10^{-3.25}), (0.15, 10^{-3.25})$, and $(0.05, 10^{-3.25})$ with $R_0 = 0.41, 0.20, 0.81, 0.2$ for Apurimac, Cajamarca, Lima, and Madre de Dios, respectively.

S4.3 β_N versus β_R

Our model includes two infectious classes: the I_N class in which bats can transmit rabies but their infections are subclinical, and the I_R class in which bats have developed clinical symptoms. Therefore, we assumed that the corresponding transmission rates β_N and β_R can differ between these classes because of, for example, differences in contact rates resulting from behavioral changes after a bat develops clinical rabies. Specifically, as with other animals both furious and paralytic forms of disease are possible. Furious animals actively seek and bite other individuals, while animals with the paralytic form may be withdrawn, lethargic and irritable, but may still bite in response to normal social interactions among bats. Each of these forms of disease are included in the I_R class. Non-rabid transmission between bats, the I_N class, is expected to be the less important form of transmission among bats, but may still occur when saliva is transferred through fighting, allo-grooming or perhaps through regurgitation of blood between individuals during food sharing. Non-rabid transmission, however, is critically important for transmission to humans and livestock since bats in this class excrete virus in their saliva, but feed normally, thus exposing their prey to rabies virus during feeding events.

Here, we describe the relationship between the transmission rates β_N and β_R. For illustrative purposes we only show the results for model I, but each model tested results in similar relationships. Using a relatively low effect of immigration, we observed that the optimal transmission rates β_N and β_R strongly depend on the intrinsic basic reproductive ratio, R_0 (Figure S7-A). Specifically, for a given infection probability (α) and contribution of immigration to the force of infection (ϕ), the relative magnitude of β_N and β_R are nearly indistinguishable given that the appropriate R_0 is attained (Figure S7-A,C). Importantly, by increasing the level of immigration we find that as the level of immigration increases, lower transmission rates are favored which in turn decreases the intrinsic R_0 (Figure S7-B). Further, we note that while immigration ϕ is smaller than the MLE, the optimal value of α tends to decrease as ϕ increases (from 0.35 to 0.1, respectively; see also Fig. S8). This relationship is intuitive: the infection probability must decrease with greater rabies exposure resulting from immigrating bats – otherwise, the population would ultimately be driven to extinction.

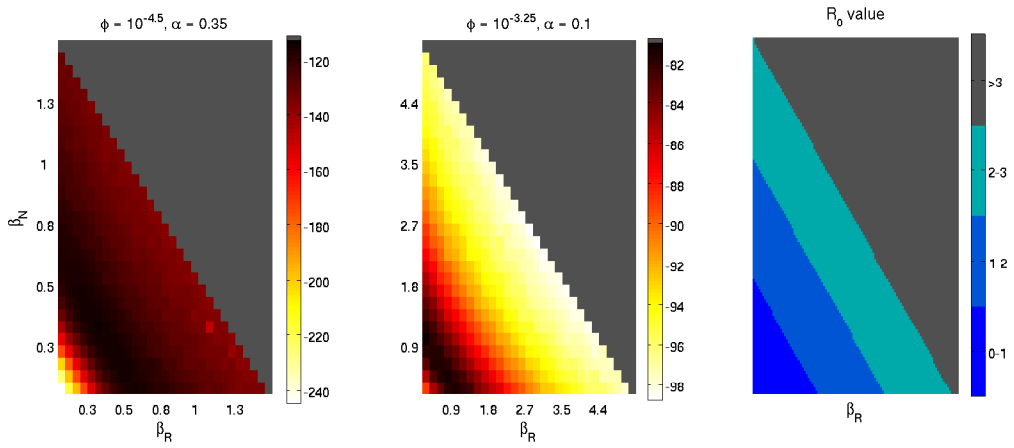

Figure S7. (Left, middle) Plots of the log likelihood value for β_N versus β_R for two values of the effect of transmission $(10^{-4.5}, 10^{-3.25})$. Infection probability α is fixed at the corresponding maximum likelihood estimate for the given ϕ. (Right) Associated intrinsic R_0 values. In all plots, dark gray indicates that $R_0 > 3$. This figure demonstrates that the relationship between β_R and β_N only requires that the appropriate R_0 is attained.

S5 Derivation of R_0

We computed the intrinsic R_0 value – or the basic reproductive ratio in the absence of immigration – for each model I-IV using the next generation matrix ([18, 19]). For models I, III, and IV, we find that

$$R_0 = \alpha \left(\beta_N \frac{1}{(\tau_2 + \mu)} \frac{\tau_1}{(\tau_1 + \mu)} + \beta_R \frac{1}{(\delta + \mu)} \frac{\tau_1}{(\tau_1 + \mu)} \frac{\tau_2}{(\tau_2 + \mu)} \right).$$

The resulting sum is multiplied by α, or the fraction of individuals developing lethal infection following exposure. The first two elements of each term in the sum are the infection rate times the infectious period for I_N and I_R, respectively. The additional element in the first term of the sum discounts R_0 by the death of individuals in the exposed class who do not contribute to the chain of transmission; similarly, the second term in the sum discounts R_0 by the death of exposed individuals multiplied by the death of individuals in I_N who do not contribute to the chain of transmission in I_R.

Model II, which allows for recovery from the infectious class that has not yet developed clinical symptoms (I_N), has an additional term in the R_0 value representing the proportion of individuals who remain in the I_N class following infection (ρ) so that

$$R_0 = \alpha \left(\beta_N \frac{1}{(\tau_2 + \mu)} \frac{\tau_1}{(\tau_1 + \mu)} + \beta_R \frac{1}{(\delta + \mu)} \frac{\tau_1}{(\tau_1 + \mu)} \frac{\rho\tau_2}{(\tau_2 + \mu)} \right).$$

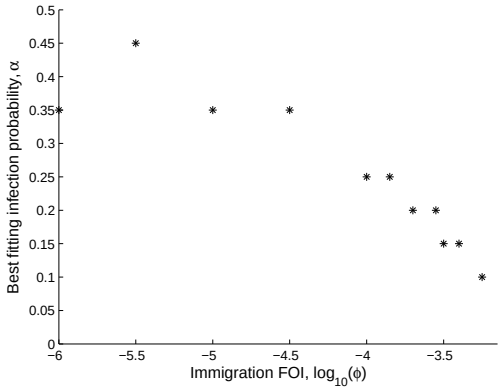

Figure S8. Scatter plot of the optimal value of α for each ϕ where ϕ is lower than the MLE. Note the decreasing trend in α as ϕ decreases.

S6 Sensitivity analysis: culling

In the main text, we provided an analysis of the change in seroprevalence and expected daily exposure rate of livestock to I_N bats following culling via vampiricide. Topical vampiricide is an anticoagulent poison (typically warfarin) that is applied in a paste to the fur of bats that are captured in the field. The treated bats are released and ingest the poison upon grooming. The paste is thought to be spread to non-treated individuals through allo-grooming [20, 21].

The main text displayed our results for culling that removed 50% of the affected population. This was accomplished by finding the mean seroprevalence over 1000 stochastic realizations in the year immediately following a cull for each study site. Here, we demonstrate that our conclusions are invariant to the percent of a bat colony effectively culled. As shown in Figure S9, for both culls of 20% and 80% we still observe only a minimal change in seroprevalence regardless of whether culling targets previously exposed bats. As demonstrated in Figure S9, this observation also holds when considering I_H prevalence only. We also again find that the exposure rate effectively changes proportional to the culling percentage when averaged over the first year post-cull.

In our model we assumed that rabies transmission is frequency dependent because of the absence of a significant relationship between seroprevalence and colony size [11]. However, if we instead assumed that transmission is density dependent so that the force of infection is given by

$$\lambda = \beta_N I_N + \beta_R I_R + \phi,$$

then transmission would decrease immediately following a cull. This is in contrast to the assumption of frequency dependence, particularly in the case of indiscriminant culling, in which transmission rates do not change immediately following a cull. However, given that the seroprevalence of infectious individuals is so low (Figure S9) the decrease in transmission is likely to be short-lived and play a minimal role in the overall effects of culling.

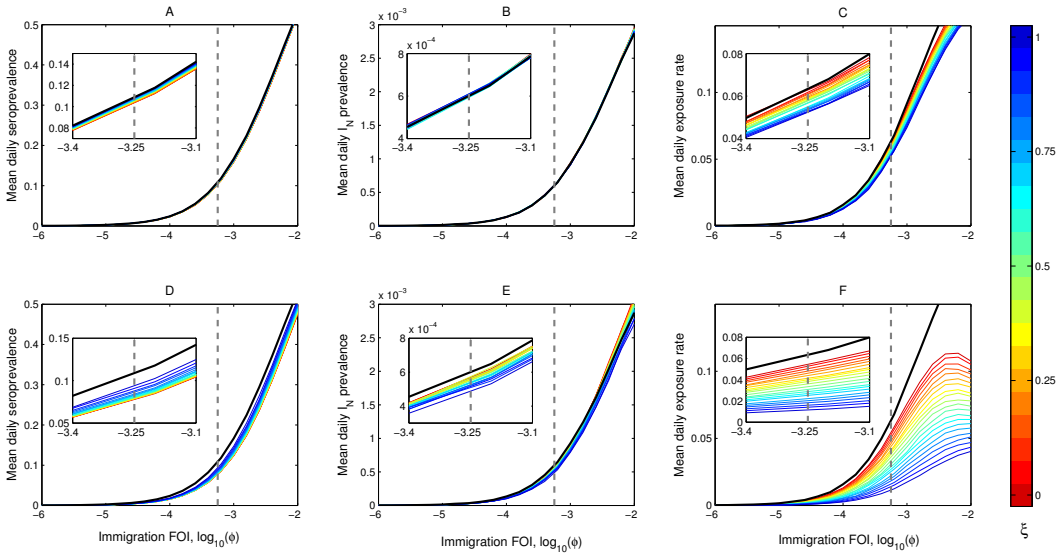

Figure S9. (**A-C**) Total seroprevalence, prevalence of I_N bats, and mean daily exposure rate averaged over the first year following a 20% cull. The dark gray dashed line corresponds to the MLE and the black line corresponds to the case of no culling. The colored lines indicate the degree of discriminant culling where dark blue is completely indiscriminate and dark red corresponds to culling directly targeted at previously exposed bats. (**D-F**) Identical to (**A-C**) with an 80% cull. Parameters are fixed at their MLE (i.e. $\alpha = 0.1$, $\phi = 10^{-3.25}$, $\beta_N = 0.3535$, $\beta_R = 0.707$

References

[1] Moreno J, Baer G (1980) Experimental rabies in the vampire bat. American Journal of Tropical Medicine and Hygiene 29: 254-259.

[2] Aguilar-Setien A, Loza-Rubio E, Salas-Rojas M, Brisseau N, Cliquet F, et al. (2005) Salivary excretion of rabies virus by healthy vampire bats. Epidemiology and Infection 133: 517-522.

[3] Almeida M, Martorelli L, Aires C, Sallum P, Durigon E, et al. (2005) Experimental rabies infection in haematophagous bats Desmodus rotundus. Epidemiology and Infection 133: 523-527.

[4] Ionides E, Bretó C, King A (2006) Inference for nonlinear dynamical systems. Proc Natl Acad Sci U S A 103: 18438-18443.

[5] King A, Ionides E, Bretó C, Ellner S, Kendall B (2009). POMP: statistical inference for partially observed markov processes (R package). URL `http://pomp.r-forge.r-rproject.org`.

[6] Gillespie D (1976) General method for numerically simulating stochastic evolution of coupled chemical-reactions. J Comput Phys 22: 403-434.

[7] Gillespie D (1977) Exact stochastic simulation of coupled chemical reactions. J Phys Chem 81: 2340-2361.

[8] Gillespie D, Petzold L (2003) Improved leap-size selection for accedlerated stochastic simulation. J Chem Phys 119: 8229-8234.

[9] Lord R (1992) Seasonal reproduction of vampire bats and its relation to seasonality of Bovine rabies. Journal of Wildlife Diseases 28: 292-294.

[10] Wilkinson G (1985) The social organization of the common vampire bat: Ii. Mating system, genetic structure, and relatedness. Behavioral Ecology and Sociobiology 17: 123-134.

[11] Streicker D, Recuenco S, Valderrama W, Gomez-Benavides J, Vargas I, et al. (2012) Ecological and anthropogenic drivers of rabies exposure in vampire bats: implications for transmission and control. Proceedings of the Royal Society B: Biological Sciences 279: 3384-3392.

[12] Jackson A, Randle E, Lawrance G, Rossiter J (2008) Neuronal apoptosis does not play an important role in human rabies encephalitis. Journal of Neurovirology 14: 368-375.

[13] Turmelle A, Allen L, Jackson F, Kunz T, Rupprecht C, et al. (2010) Ecology of rabies virus exposure in colonies of Brazilian free-tailed bats (*Tadarida brasiliensis*) at natural and man-made roosts in Texas. Vector-borne and Zoonotic Diseases 10: 165-175.

[14] Lord R (1976) Salud animal: programa y tendencias en las Americas, Publicacion Cientifica No 334, Washington, DC: Organizacion Panamericana de la Salud, chapter Importancia de los murcielagos en la epidemiologia de las zoonosis, con enfasis en la rabia bovina. pp. 89-97.

[15] Wilkinson G (1984) Reciprocal food sharing in the vampire bat. Nature 308: 181-184.

[16] Turner D (1975) The vampire bat: a field study in behavior and ecology. Baltimore, MD: The Johns Hopkins University Press, 145 pp.

[17] Turmelle AS, Jackson FR, Green D, McCracken GF, Rupprecht CE (2010) Host immunity to repeated rabies virus infection in big brown bats. Journal of General Virology 91: 2360-2366.

[18] Diekman O, Heesterbeek J, Metz J (1990) On the definition and the computation of the basic reproduction ratio r_0 in models for infectious diseases in heterogeneous populations. Journal of Mathematical Biology 28: 365-382.

[19] van den Driessche P, Watmough J (2002) Reproduction numbers and sub-threshold endemic equilibria for compartmental models of disease transmission. Math Biosci 180: 29-48.

[20] Linhart S, Crespo R, Mitchell G (1972) Control of vampire bats by topical application of an anticoagulant, chlorophacinone. Bol of Sanit Panam 6: 31-38.

[21] Gomes M, Uieda W, Latorre M (2006) Influence of sex differences in the same colony for chemical control of vampire *Desmodus rotundus* (phyllostomidae) populations in the state of Sao Paulo, Brazil. Pesq Vet Bras 26: 38-43.